Immunological Synapse Dynamics Induced by Bispecific T-cell Engagers Predict Clinical Pharmacodynamics and Tumor Evolution across Anatomical Sites

Can Liu[1], Jiawei Zhou[1], Stephan Kudlacek[2], Timothy Qi[1], Tyler Dunlap[1], Yanguang Cao[1,3]

[1]Division of Pharmacotherapy and Experimental Therapeutics, School of Pharmacy, University of North Carolina at Chapel Hill, NC 27599, USA; [2]Department of Biochemistry and Biophysics, University of North Carolina at Chapel Hill, NC 27599, USA; [3]Lineberger Comprehensive Cancer Center, School of Medicine, University of North Carolina at Chapel Hill, NC 27599, USA.

Corresponding author:

Yanguang Cao, Ph.D.

Division of Pharmacotherapy and Experimental Therapeutics, UNC School of Pharmacy

2318 Kerr Hall, UNC Eshelman School of Pharmacy

Chapel Hill, NC 27599-7569

E-mail: yanguang@unc.edu

Phone: +1-919-966-4040.

Abstract

Bispecific T cell engagers (BiTEs) engage T cells for anti-tumor activity. Despite early successes such as blinatumomab, the therapeutic potential of BiTEs for cancer immunotherapy remains limited by low response rates and high potential for relapse. Formation of the immunological synapse (IS) is principal to BiTE pharmacology and BiTE-directed lysis of tumor cells by T cells. Unfortunately, our knowledge of BiTE-induced IS formation dynamics and its relation to treatment resistance remains rudimentary. This work develops an integrated experimental and theoretical approach to investigate IS formation dynamics induced by BiTEs under diverse conditions. Our theoretical models recapitulate experimental observations by defining IS formation as spatiotemporally coordinated events driven by molecular and cellular interactions. These models adequately predicted tumor-killing profiles in patients and revealed a trajectory of antigen escape and tumor evolution across anatomical sites, particularly highlighting the role of the bone marrow in disease relapse. Our work yields implications for developing more effective cancer immunotherapies.

Introduction

Cancer immunotherapy has become a mainstream therapeutic for many types of cancer. Bispecific T cell engagers (BiTE) are a unique type of cancer immunotherapy. Despite early successes, many challenges remain for BiTE immunotherapy; only a fraction of patients respond and many responders eventually relapse[1-3]. BiTEs redirect T cells to bind specific antigens on tumor cells and facilitate the formation of immunological synapses (IS) through tight intercellular apposition, leading to cytolysis of the tumor cell. IS formation therefore is an indispensable component of BiTE pharmacology[1]. Like the IS between antigen-presenting cells and T cells, the BiTE-induced IS formed between tumor cells and T cells is also a precisely orchestrated cascade of molecular and cellular interactions[4,5]. Understanding the dynamics of IS formation and the factors governing the process is vital to characterizing BiTE pharmacodynamics and mechanisms of treatment resistance.

The molecular basis of IS formation has been widely studied to inform potential molecular targets for cancer immunotherapy[6,7]. However, the entire macroscopic process of IS formation goes beyond molecular crosslinking and entails multiple intercellular interaction steps, such as T cells scanning of target cells in tumor microenvironment, slowing their motility upon recognition, and establishing intercellular adhesion in response to signals generated at the first encounter[8,9]. Previous pharmacodynamic models of BiTE immunotherapy have almost exclusively focused on the molecular crosslinking steps, with little consideration of macroscopic intercellular interactions[10-13]. We sought to investigate if these intercellular interactions are essential for predicting IS formation dynamics.

Tumor cells reside in dynamic and heterogeneous microenvironments. Suboptimal BiTE efficacy can result from insufficient effector cell numbers, poor drug penetration into tumor, and immune escape. Characterizing IS formation dynamics under diverse conditions, such as varying T cell densities, BiTE concentrations, antigen binding affinity, and target antigen expression, would provide insights into BiTE pharmacodynamics and reveal possible treatment resistance mechanisms. Bell. et al. developed theoretical models of cell-cell adhesion[14] that highlighted not only the importance of cell-surface receptors and ligands, but also biophysical factors including receptor diffusivity on the cell membrane and hydrodynamic shearing forces. So far, the dynamics

of IS formation induced by BiTEs in cell population remains understudied, limiting knowledge of BiTE efficacy in various environments.

In this study, we applied imaging flow cytometry to quantify BiTE-induced IS formation dynamics under varied experimental conditions. In parallel, we developed theoretical models to simulate IS formation on different spatiotemporal scales and interrogate factors influential to this process. After considering patient-specific parameters, models incorporating IS formation dynamics adequately predicted tumor-killing profiles in patients. These models revealed trajectories of antigen escape and tumor evolution across anatomical sites that have substantial implications for the development of more effective T cell-based cancer immunotherapies.

Results

Experimental design and theoretical models

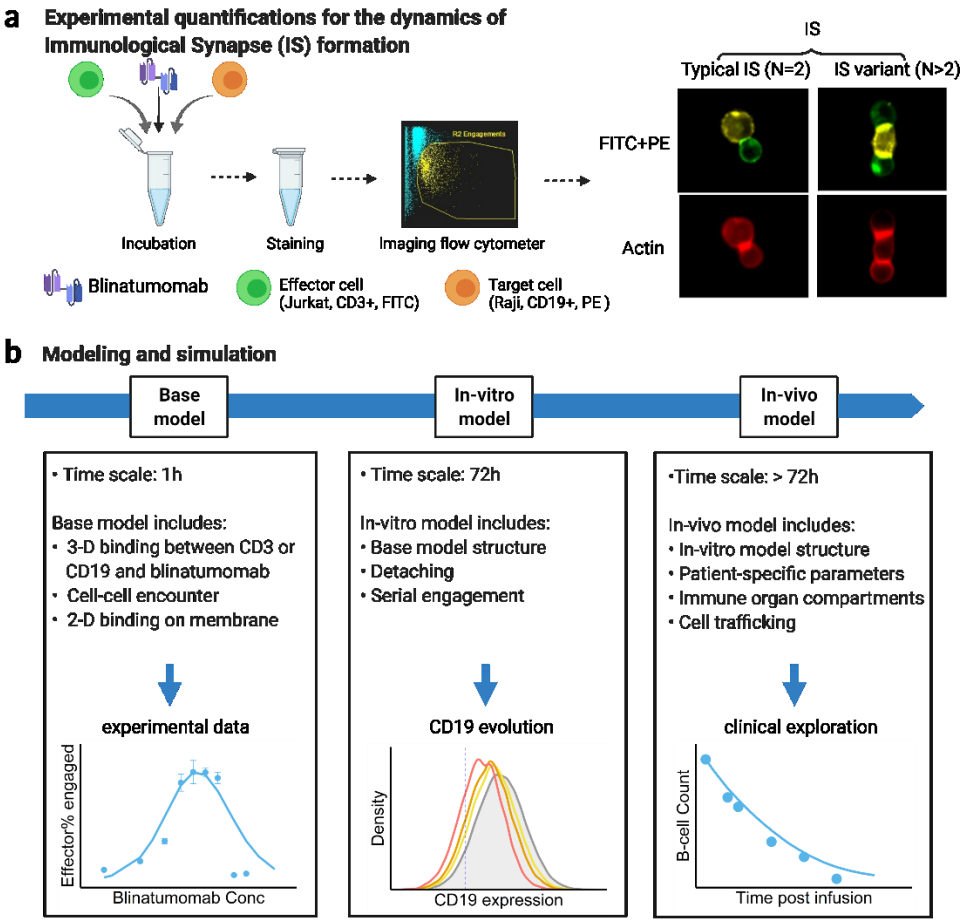

Figure 1. Schematic of experimental design and theoretical models. The study examined the formation dynamics of immunological synapses (IS) elicited by a bispecific T cell engager (BiTE). **a** the abundance and dynamics of IS formation were quantified by imaging flow cytometry under various experimental conditions. **b** three mechanistic agent-based models were developed for comprehensive characterizations of cell-cell engagement and tumor-killing effects on different spatiotemporal scales. 3-D, three-dimensional; 2-D, two-dimensional.

IS and the dynamics of IS formation were the focus of this study. As depicted in Fig. 1a, $CD3^+$ Jurkat were used as effector cells (E) while $CD19^+$ Raji were used as target cells (T). Jurkat and Raji cells were sorted into three subpopulations, high (H), medium (M), and low (L), based on their membrane expressions of CD3 or CD19, respectively (Supplementary Fig. S1). Effector and

target cells were co-incubated in the presence of blinatumomab. IS formation dynamics were visualized and quantified by imaging flow cytometry (Fig. 1a and Supplementary Fig. S2). We quantified the dynamics of IS formation under various experimental conditions, including different cell densities, antigen expressions, incubation durations, E:T ratios, and antibody concentrations. Multiple types of IS were observed and quantified, including typical IS with one effector and one target cell (ET) and IS variants with three or more cells engaged, such as ETE, ETT, ETET.

We developed three mechanistic agent-based models to investigate IS formation and the resultant tumor-killing on different spatiotemporal scales. Three models were developed in a step wise fashion and calibrated with the respective data. As shown in Fig. 1b, the base model was developed for predicting IS formation dynamics within 1 hour. The base model consists of three fundamental components during IS formation: three-dimensional (3D) binding between antibody and target antigens (CD3 or CD19) to form binary complexes, the probability of cell-cell encounter, and cell-cell adhesion driven by two-dimensional (2D) binding to form ternary complexes (CD3-BiTE-CD19) on the cellular membrane. Model structure and assumptions are provided in Fig. 2 and the method section (Supplementary Fig. S3-S9, and Supplementary Table S1-3).

Next, the base model was extended with serial cell-cell engagement dynamics to capture IS formation and tumor-killing up to 72 hours; we refer to this as the in-vitro model. The in-vitro model could evaluate the chance for antigen escape (i.e., CD19 escape), a common mechanism of tumor resistance to BiTEs[2,3].

Last, the in-vitro model was expanded to include cell-cell engagement in anatomically distinct compartments in the body. This model considered the infiltration gradients of T and B cells and organ-to-organ cell trafficking. We refer to this expanded model as the in-vivo model. The in-vivo model could integrate patient-specific parameters (Supplementary Table S2, S3) to predict the clinical profiles of tumor killing and relapse. The in-vivo model was also applied to support simulation of antigen escape and tumor evolution in space.

Model structure

The major mechanism of action of BiTEs is to produce ternary complexes (CD3-BiTE-CD19) on opposing cell surfaces, driving IS formation. In this study, we found the dynamics of IS formation to be, essentially, two independent and indispensable cellular processes mediated by cell-cell

encounter and cell-cell adhesion. Compared to molecular scale-focused pharmacodynamics models of BiTEs[10-13], our models highlight the importance of these two cellular processes for IS formation in the context of macroscopic and biophysical forces (Fig. 2).

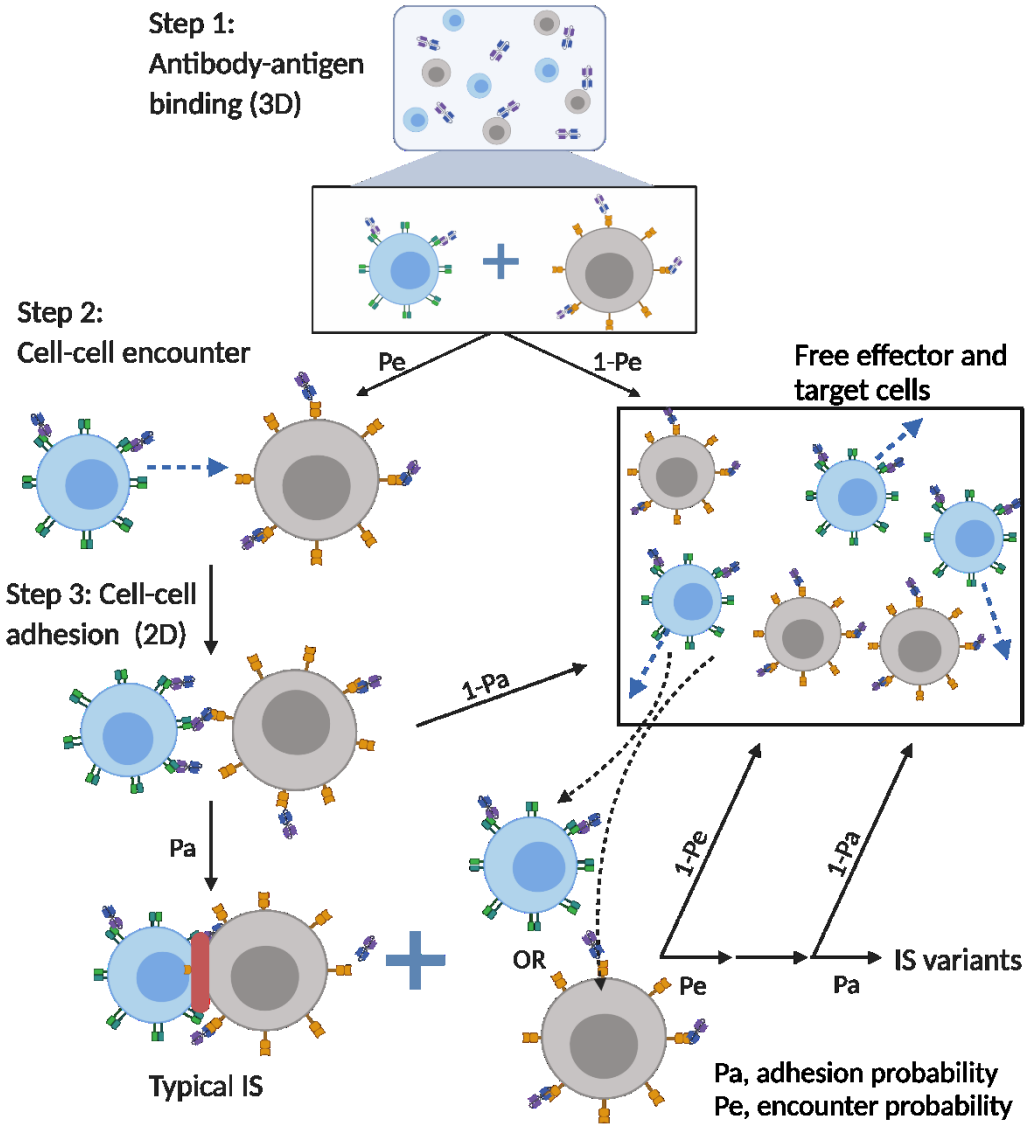

Figure 2. The base model included three essential steps to describe the process of IS formation induced by BiTEs. Step 1: three-dimensional (3D) antibody-antigen binding in the media to form a binary complex; Step 2: cell-cell encounter, with encounter probability (Pe) dictated by cell motility and density; Step 3: cell-cell adhesion and IS formation, with adhesion probability (Pa) driven by the density of ternary complexes formed on the cell-cell contact area (two-dimensional (2D) binding) during contact. Newly formed binary IS had a chance to engage additional free effector or target cells to form an IS variant.

In the base model (Fig. 2), three essential steps are defined: antibody-antigen binding to form binary complex (BiTE-CD3 and BiTE-CD19) (step 1), effector-target cell encounter and the encounter probability as a function of cell mobility and density (step 2), and effector-target cell adhesion probability as a function of ternary complexes formed during contact (step 3). Model equations are provided in Supplementary Fig. S3-S9. Antibody-antigen binding to form binary complexes (BiTE-CD3 and BiTE-CD19) were assumed to be 3D processes that reached rapid equilibrium prior to cellular-scale events. Free effector cells were assumed to follow Brownian motion and encounter target cells at a probability informed by cell density and motility in the incubation environment[15] (Fig. 2).

After cell-cell encounter, the probability of adhesion was modeled to increase as a function of the number of ternary complexes (CD3-BiTE-CD19) formed between cells during the duration of contact. Cell-cell complexes with a high number of ternary complexes would therefore have a higher probability to adhere and eventually form IS. Ternary complex formation on opposing cells was assumed to be restricted to the cell membrane (2D binding, Supplementary Fig. S6). The derivation of 2D binding affinities is provided in Supplementary Fig. S8. Cells that failed to adhere upon encounter (futile contact) were assumed to diffuse away and become free to repeat the same process. Newly formed typical IS were also modeled as being capable of engaging additional effector or target cells to become an IS variant, per our observations (Fig. 2). The model considered IS variants comprising up to 4 cells.

Effect of BiTE concentrations, cell densities, and antigen expressions on IS formations

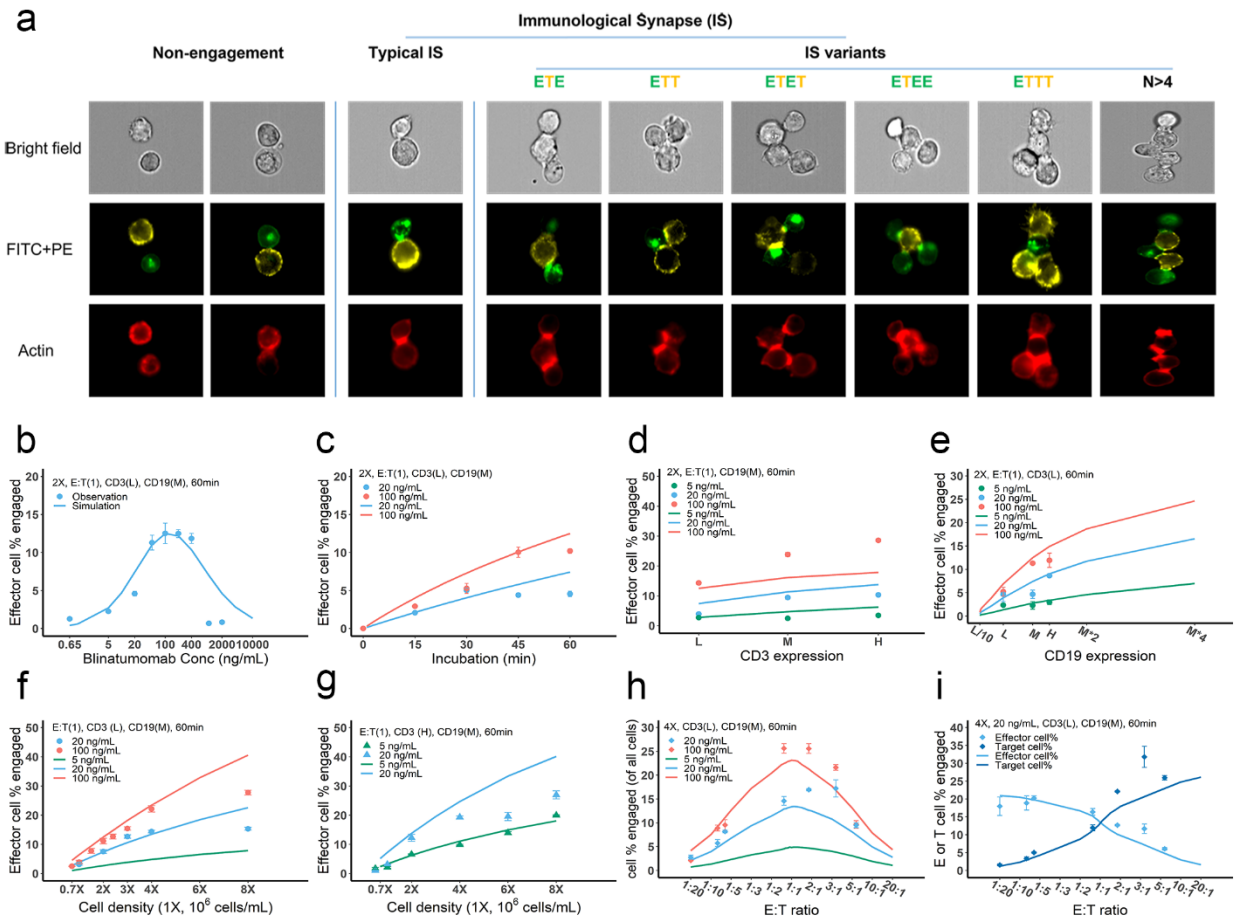

Figure 3. Dynamics of immunological synapse (IS) formation induced by BiTE under different conditions. **a** representative image of non-engagement (futile encounter), binary IS, and other IS variants. Green (FITC), effector cells (E); Yellow (PE), target cells (T). **b-i**, the effects of drug concentration (**b**), incubation duration (**c**), antigen density (**d, e**), cell density (**f, g**) and E:T ratio (**h, i**) on IS formation. Observations were dots (with SE) and model simulations were solid curves. The base model was applied to simulate IS formation under different conditions. 2X, 2×10^6 cells/mL; E:T(1), E:T ratio = 1; CD3(L), CD3 expression (Low); CD3(H), CD3 expression (High); CD19(M), CD19 expression (medium); 5, 20, 100 ng/mL, antibody concentration; 60 min, incubation duration.

IS formation dynamics were quantified by imaging flow cytometry. Representative images of non-engaged (futile contact), typical IS, and multiple IS variants are shown in Fig. 3a. IS formation required definitive contact between effector and target cells as evaluated in brightfield and FITC + PE channels. Formation of IS was determined by a high intensity of actin (red) at the contact site due to F-actin polymerization and concentration during cell adhesion[9].

To investigate the key influential factors, we evaluated IS formation under multiple experimental BiTE concentrations (0.65 – 2000 ng/ml), incubation durations (0 – 60 min), antigen densities (three levels for either CD3 or CD19), cell densities (0.7 – 8 million), and E:T ratios (0.05 – 6) (Fig. 3b-i). The fractions (%) of effector cells engaged in IS were quantified to inform IS formation dynamics. We also ran these experiments virtually using the base model to test the model predictability and explore mechanistic hypotheses.

In Fig. 3b-i, the observations (symbols) and model simulations (lines) overlapped, indicating good base model performance. IS formation exhibited a bell-shaped profile as BiTE concentrations increased in vitro (Fig. 3b). The model also predicted this bell-shaped relationship and revealed that high BiTE concentrations (> 100 ng/ml) reduce formation of ternary complexes, partly because individual antigens (CD3 and CD19) were almost completely occupied by one arm of the BiTE, thereby limiting crosslinking on opposing cells (Supplementary Fig. S6). IS formation increased over time and plateaued around 60 min (Fig. 3c). We therefore restricted our incubation to 60 min considering IS quantification could be biased by serial cell-cell engagements and potential cell lysis[8].

The effect of CD3 expression on IS formation was relatively small, especially at low BiTE concentrations (Figure 3d). The model revealed only a small fraction of CD3 was occupied; therefore, we concluded that CD3 expression not a key driver of IS formation at low BiTE concentrations. In contrast, we found CD19 expression on target cells to profoundly impact IS formation (Fig. 3e). This was also predicted by the base model.

Our model predicted that cell density would also be critical to IS formation on a per-cell basis. Increasing total cell density (E+T) from 1 to 8 million per ml at an E:T ratio around 1:1 drastically boosted IS formation from 3.1% to 15.3% at 20 ng/ml BiTE and 3.9% to 27.8% at 100 ng/ml BiTE. IS formation was further increased with high CD3-expressing effector cells at high cell densities (Fig. 3g).

The E:T ratio also played a pivotal role in IS formation. IS formation was optimal when the E:T ratio was around 1 (Fig. 3h). Changing the E:T ratio led to variations in the fraction of effector and target cells that involved in IS formation, as predicted by the model. With higher E:T ratios, a greater fraction of target cells but a lower fraction of effector cells were involved in IS formation (Fig. 3i and Supplementary Fig. S10).

Overall, we found multiple factors to be influential to IS formation. The model reasonably recapitulated IS formation dynamics under various conditions (Fig. 3b-i and Supplementary Fig. S10). The goodness of model predictions is provided in Supplementary Fig. S11. With good model predictability, we further investigated the influence of CD3 and CD19 binding affinities. Counterintuitively, higher affinities to CD3 resulted in lower predicted IS formation, perhaps due to higher degrees of CD3 downregulation (Supplementary Fig. S12a). Reduced IS formation at high CD3 affinities also resulted in a bell-shaped relationship (Supplementary Fig. S12b). Notably, the approved BiTE blinatumomab is in the optimal range of affinity to CD3. BiTEs with higher affinity to CD19 could considerably enhance IS formation (Supplementary Fig S12c, d).

IS variants were prevalent and well predicted by the base model

Many types of IS variants were observed in the experimental system. In total, six types of IS were quantified, including binary IS, ETE, ETT, ETET, ETEE, and ETTT. The IS variants with more than 4 cells were not analyzed in our study, nor included in the base model, due to their low abundance. The frequency of these variants was recorded and compared under each experimental condition.

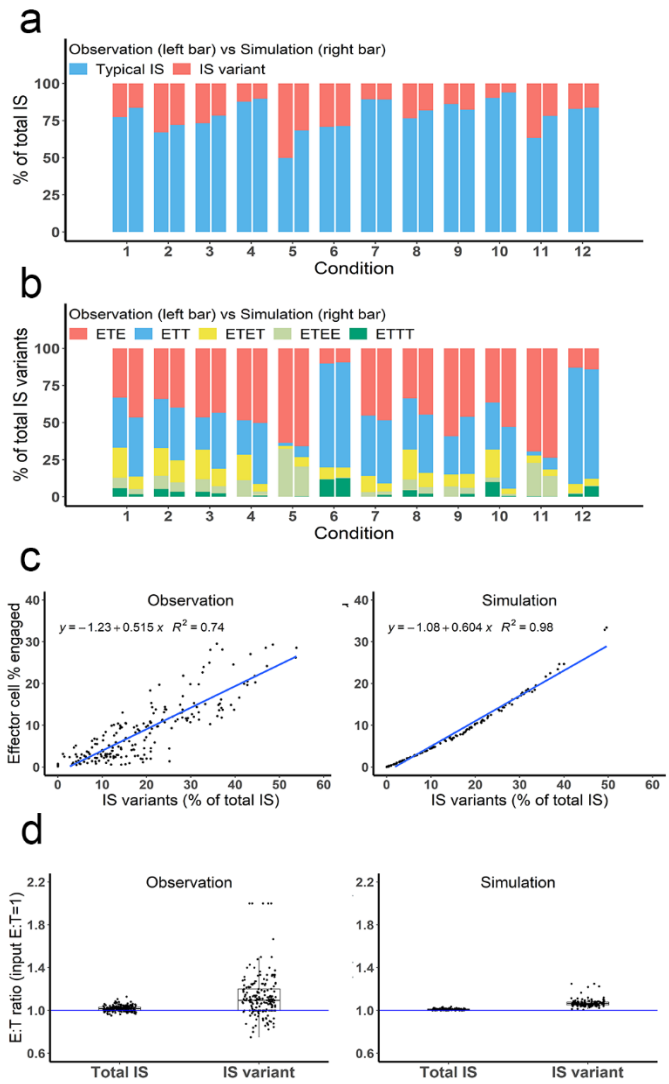

Figure 4. Multiple types of IS variants were observed and well predicted by the base model. In total, six types of IS were quantified, including typical IS, ETE, ETT, ETET, ETEE, and ETTT. **a** the fraction of typical IS and variants under different conditions; **b** the composition of IS variants (ETE, ETT, ETET, ETEE, ETTT) under different conditions; **c** the positive correlation between the fraction of IS variants (% of total IS) and total IS formation (effector cell % engaged). The formula and R^2 of linear regressions are shown. **d** the E:T ratios involved in total IS and IS variants. Experimental setup: Condition 1, 2X, E:T(1), CD3(L), CD19(M), 100 ng/mL, 60 min; Condition 2, 4X, E:T(1), CD3(L), CD19(M), 100 ng/mL, 60 min; Condition 3, 2X, E:T(1), CD3(H), CD19(M), 100 ng/mL, 60 min; Condition 4, 2X, E:T(1), CD3(L), CD19(L), 100 ng/mL, 60 min; Condition 5, 4X, E:T(6), CD3(L), CD19(M), 100 ng/mL, 60 min; Condition 6, 4X, E:T(0.17), CD3(L), CD19(M), 100 ng/mL, 60 min; Conditions 7-12 are the same as Conditions 1-6, except with lower BiTE concentrations (20 ng/mL).

Depending on the experimental conditions, approximately 12 - 25% of IS observed were IS variants, up to 50% under condition 5 due to high cell density and BiTE concentration (Fig. 4a). Among these IS variants, ETE and ETT were the most frequently observed, accounting for more than 60% of total IS variants formed under all conditions. Conditions 5 and 11 showed high ETE frequencies due to a high E:T ratio (6:1), while conditions 6 and 12 showed high ETT frequencies due to a low E:T ratio (1:5.8). The base model well predicted the relative fraction of each IS variant under all tested conditions (Fig. 4a). In general, the fraction of IS variants increased with total IS abundance. The positive correlation between the fraction of IS variants and effectors cells involved in IS were well predicted by the base model (Fig. 4c)

The E:T ratios of all IS variants were pooled for comparison (Fig. 4d). The median E:T ratio in total IS was about 1.0. When excluding typical IS, this ratio increased to 1.1 for the remaining IS variants, suggesting slightly more effector cells involved in IS variant formation than target cells, in line with model predictions.

The in-vitro model predicted antigen escape and organ reservoirs

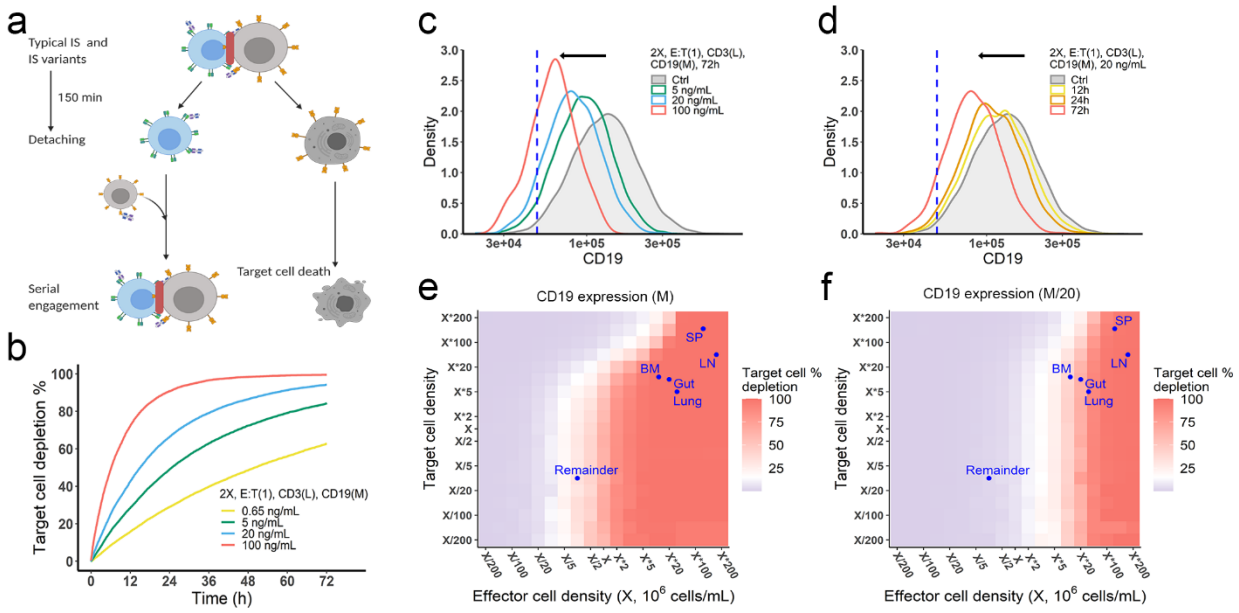

Figure 5. Exploration on mechanism of drug resistance by the in-vitro model. **a** scheme of cell detaching and serial engagement in the in-vitro model; **b** long-term simulation (72h) on target cell depletion across drug concentrations; **c, d** the effects of drug concentration (**c**) and incubation time (**d**) on CD19 evolution. Dashed line, pre-defined threshold value of CD19 expression for 15% target cell depletion within 72h (initial setup: 2X, E:T(1), CD3(L), 0.65 ng/mL, 72h). Ctrl, initial

CD19 distribution in target cell population. **e, f** the effects of effector and target cell density on target cell depletion (%). White, 15% target cell depletion. Initial setup: CD3(L), CD19(M) for (**e**), CD19 (M/20) for (**f**), 0.65 ng/mL, 72h.

Effector cells detach from IS and re-engage with other target cells in a process called serial cellular engagement. These effector cells are also known as serial killers[8,16]. We extended the base model to incorporate IS detachment and re-engagement (Fig. 5a). The in-vitro model simulated IS formation and cellular cytotoxicity up to 72 hours. With serial engagement and killing, the fraction of target cell lysis increased considerably even at low BiTE concentrations (Fig. 5b).

Importantly, the in-vitro model predicted tumor evolution toward populations with low CD19 expression (i.e., antigen escape). As shown in the model, tumor cells with lower CD19 expression had a lower chance of being engaged by effector cells and thus a higher probability of surviving (Fig. 5c, d). The speed of evolution was predicted to increase at greater BiTE concentrations (Fig. 5c) and become more apparent over time (Fig. 5d). The effects of other factors, such as cell density and antigen affinity, on tumor evolution were also simulated (Supplementary Fig. S13). Of note, the higher the formation of IS, the more extensive the evolution toward lower CD19-expressing cells.

The impact of cell density at clinically relevant BiTE concentrations was also interrogated (Fig. 5e, f and Supplementary Fig. S14). Notably, an increase of effector cell density resulted in higher fractions of target cell lysis at 72 hours. However, a higher density of target cells did not markedly diminish the fraction of target cells lysed at a given effector cell density, due to a compensatory increase in the probability of cell-cell encounter probability per effector cell. When target cell density was extremely high (e.g., $> 5\times10^6$/mL with CD19 expression at 1.4×10^5/cell), lysis fraction decreased, as the low BiTE concentration may have become a limiting factor for IS formation. We compared organ-specific effector and target cell abundance to show the predicted gradient of cell lysis across organs (Fig. 5e, f and Supplementary Fig. S14). Higher target cell lysis was predicted in lymph nodes and the spleen due to their rich effector cells. The bone marrow and remainder (most non-lymphoid) organs showed restricted cell lysis primarily due to the low abundance of effector cells (Fig. 5f). The model also predicted that some organs like the bone marrow may become tumor cell sanctuary sites, conferring space for tumor adaptation and survival and thereby increasing the likelihood of tumor resistance.

The in-vivo model predicted clinical outcomes and tumor evolution across anatomical sites

We developed the in-vivo model by defining IS formation dynamics in organs and cell trafficking across organ compartments (Fig. 6a). We used the model to simulate cell lysis in each organ and tumor-killing profiles throughout the body. Organ-specific cell lysis is highly dependent on relative IS formation dynamics and thus is a function of organ-specific effector (T cell) and target (B cell) populations and BiTE exposure.

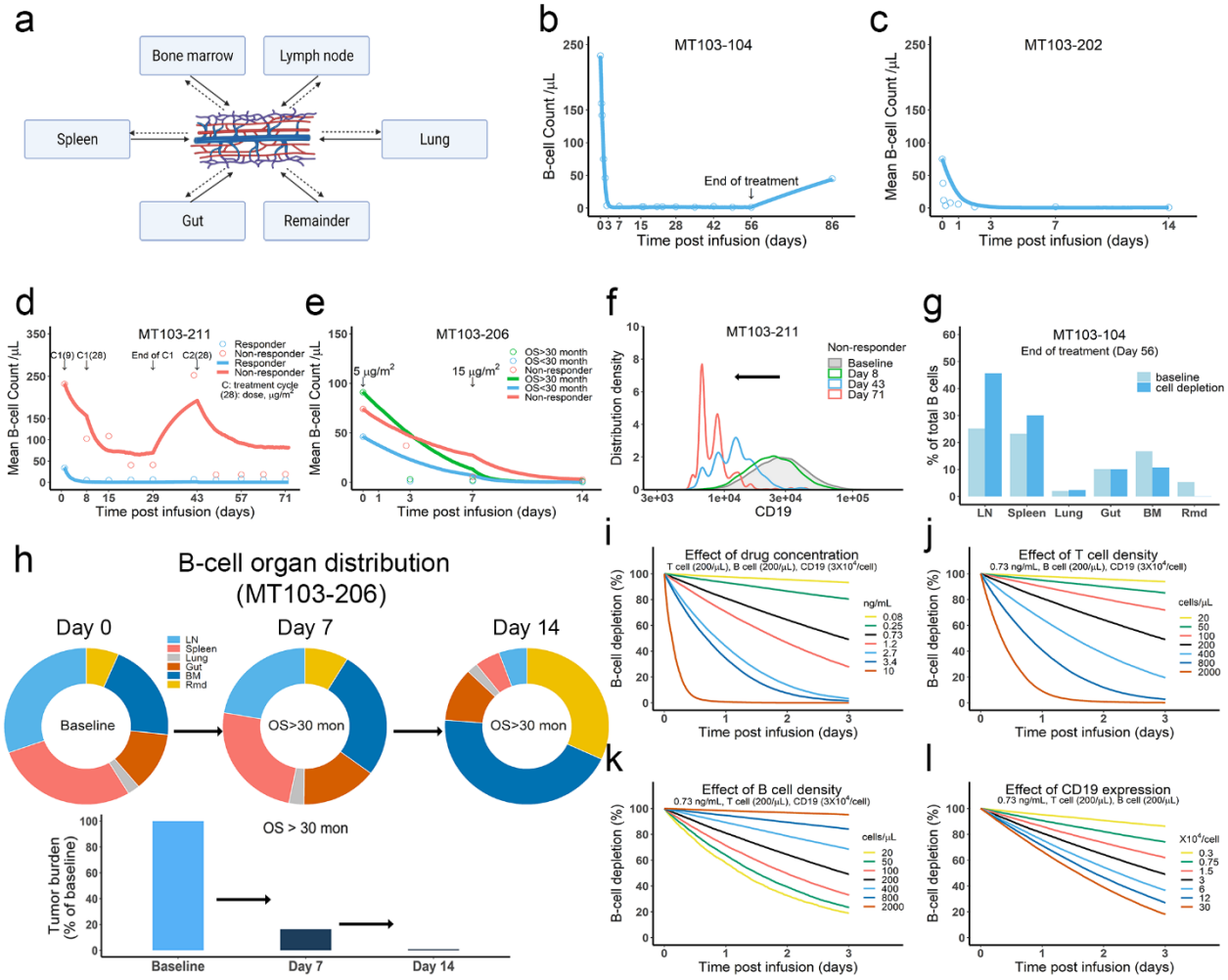

Figure 6. Clinical translation and exploration with the in-vivo model. **a** scheme of organ compartment and cell trafficking; **b-e** observed and simulated patient B-cell profiles in blood. For trial information and parameters, see Supplementary Table S2,3; **f** simulated CD19 evolution in non-responder patients of trial MT103-211; **g** simulated cell lysis potency for each organ in trial MT103-104; **h** simulated baseline (Day 0), and post-treatment (Day 7 and 14) B-cell organ distribution in patients with OS > 30 month of MT103-206. Bar plot, simulated baseline and post-treatment tumor burden; **i-l** sensitive analyses for the impact of drug concentration (**i**), T cell density (**j**), B cell density (**k**), and CD19 expression (**l**) on B-cell depletion. OS, overall survival.

Shear stress restricts cell-cell adhesion and IS formation. Negligible IS formation was observed under shear stress forces equivalent to blood flow (Supplementary Fig. S15a). Once formed, IS in the blood are unlikely to be broken through shear stress (Supplementary Fig. S15b). Therefore, in the in-vivo model, the blood compartment serves a mere trafficking route and does not mediate IS formation and detachment (Fig. 6a). Blood B cell levels reflect the systemic average. Although only 2% of lymphocytes are present in the blood, blood flow can transport about 5×10^{11} lymphocytes each day – comparable to the total number of lymphocytes in the body[17].

Patients showed mixed responses to BiTE immunotherapy. Some patients exhibited complete tumor eradication while others had negligible responses. By adopting patient-specific parameters, such as BiTE dosing regimens and T cell proliferation profiles, the in-vivo model reasonably predicted B-cell depletion profiles in patients treated with blinatumomab in multiple clinical trials (Fig. 6b-e and Supplementary Table S2,S3). In MT103-211 and MT103-206, rapid accumulation of T cells in the blood was observed in responders but not non-responders[18,19]. The model could account for these patient-specific T cell profiles to distinguish these two patient populations (Fig. 6d, e).

Like the in-vitro model, the in-vivo model also predicted evolution toward low CD19-expressing cell populations over time, as shown in non-responders in MT103-211 (Fig. 6f). This process is inevitable; the stronger the therapeutic pressure, the lower CD19-expression in the surviving cell population. The fraction of low CD19-expressing cells increases over time while the efficiency of tumor cell lysis decreases, leading to gradual loss of drug sensitivity.

We finally explored tumor evolution across anatomical sites and characterized the spatial gradients of cell lysis. The lymph node, spleen, and lung showed higher fractions of cell lysis than the gut, bone marrows, and remainder (Fig. 6g). More than 45% of malignant cells in the system were lysed in the lymph nodes and around 30% were eradicated in the spleen. Lytic fractions were higher than their respective baseline levels in both organs, confirming enhanced tumor killing mediated by BiTE. In contrast, the lytic fraction in the bone marrow was lower under treatment than at baseline (Fig. 6g), indicating poor tumor lysis efficiency. The anatomical differences in efficiency of cell lysis affect B-cell biodistribution after BiTE treatment in patients (Fig. 6h and Supplementary S16). The relative anatomical distribution of B cells shifted considerably over time. In high responders (OS > 30 months, MT103-206), over 99% of B cells were eradicated in the

system, particularly in organs with high predicted lysis (lymph nodes and spleen). In the bone marrow, a small fraction of B cells survived, and the surviving cell populations showed considerably lower CD19 expression. Unfortunately, the surviving cell populations gradually repopulated the bone marrow, leading to B-cell rebound and eventually patient relapse. By contrast, non-responders had a lower fraction of B cell lysis by day 14, with B cell distribution profiles remaining similar to the baseline (Supplementary Fig. S16).

Sensitivity analyses confirmed that baseline tumor burden, drug concentration, cytotoxic T cell infiltration, and CD19 expression were critical to patient response (Fig. 6i-l).

Discussion.

The clinical efficacy of BiTE immunotherapy remains suboptimal despite remarkable progress, with only a fraction of patients responding and frequent disease relapse. Understanding IS formation, a crucial component of many T cell immunotherapy's mechanism of action, can yield insights into the pharmacodynamics of BiTEs and subsequent treatment resistance. This study used an experimentally and theoretically integrated approach to examine IS formation dynamics induced by BiTEs on a population level. The abundance of IS caused by BiTEs was quantified using imaging flow cytometry, and the dynamics of IS formation were simulated with theoretical models. By defining IS formation as a spatiotemporal orchestration of molecular and cellular interactions, our theoretical models recapitulated the experimental data well. Notably, the models predicted a common resistance mechanism to BiTE immunotherapy – antigen escape. Tumor cells with lower antigen expression accumulated over time, leading to treatment resistance and eventual disease relapse. The anatomical heterogeneity of T cell infiltration and E:T ratios across organs conferred varying degrees of cell lysis efficiency. In particular, tumor cells in the bone marrow are spatially protected and have a higher chance of surviving, which could fuel tumor evolution and lead to disease relapse.

IS formation induced by BiTEs is determined mainly by two cell-scale interaction processes: cell-cell encounter and adhesion. Cell-cell encounter is the first step and, in many instances, is the rate limiting to IS formation. For simplicity, the models assume cell motion is entirely random without considerations for directed or chemotactic movement[15]. Cell density is another critical factor; cell encounter probability could become the rate-limiting step for IS formation when the target cell density is extremely low that effector cells have little chance of encountering target cells. This could be particularly challenging for patients with minimal residual disease. When the effector cell density is low, as in the bone marrow, tumor cells have a higher chance of surviving for long enough to develop immune evasion mechanisms, leading to treatment resistance. On the other hand, when target cell density is extremely high within an organ, target cell lysis may be compromised by insufficient antibody concentrations conferred by a clinically utilized dose (Fig. 5e,f and supplementary Fig. S17). This is consistent with clinical observations that the efficacy of blinatumomab is much higher in patients with relatively low tumor burden.[20,21]

The molecular crosslinking between BiTEs and target antigens affects the probability of cell-cell adhesion upon encounter. Drug concentrations, binding affinity, and antigen expressions are critical determinants of this process. Many studies have reported a bell-shaped drug concentration-response profile for BiTE immunotherapy[11,12,22,23], with the primary mechanism underlying the phenomenon being the oversaturation of T cell receptors at extremely high BiTE concentrations. The theoretical model reported herein also predicts a bell-shape concentration – IS curve, but the predicted curve peaked at higher antibody concentrations if not including the possibility of CD3 down-regulation by effector cells upon antibody engagement. Our models suggest that blinatumomab has affinity for CD3 within the optimal range.

We explored the different effects of CD19 on cellular and molecular processes. Total CD19 in the system was jointly influenced by CD 19 expression on membrane and target cell density. CD19 expression influenced cell lysis to a similar extent as target cell density when both factors were low (Supplementary Fig S17a). However, an increase of CD19 expression beyond 1.45×10^4 receptor/cell did not further improve cell lysis. In contrast, target cell densities seemed to have a bidirectional effect on cell lysis. At low levels, escalating cell densities enhanced the probability of cell-cell encounter, while at high target cell densities (e.g. in some organs), antibody drugs concentrations were insufficient to mediate meaningful IS formation, resulting in fewer cell-cell adhesion events and less cell lysis (Supplementary Fig S17a, b). This is consistent with clinical simulations (Supplementary Fig. S17c). The different roles of CD19 expression and target cell density highlight the importance of cellular-scale interactions to IS formation that cannot be appropriately described by molecular crosslinking alone. Because of these cellular processes, our theoretical models fundamentally differ from previous BiTE pharmacodynamics models that merely consider molecular crosslinking[10-13]. In our models, molecular crosslinking caused by BiTE-induced ternary complexes drove cell-cell adhesion events, whereas cell-cell encounters were modeled as an independent process.

Heterogeneity of CD19 antigen expression is a critical factor to BiTE-induced IS formation. Target cells with lower antigen expression had a lower probability of adhesion to T cells and thus a greater chance of survival. The theoretical models suggest that tumor evolution is an inevitable consequence to treatment, and that the stronger the therapeutic selection pressure, the more tumor

cells evolve away from their pretreatment phenotype. Ultimately, the surviving tumor cells shift toward a low antigen expression population in a process known as antigen escape. Antigen escape is a common mechanism of resistance to T cell-based immunotherapy[3,24]; however, the speed of tumor evolution toward antigen escape remains hard to predict. Through defining the formation of IS, our models show a proof of concept for predicting the trajectory of antigen escape based on baseline antigen expression.

Non-uniform tumor lysis effect across organs represents another barrier for therapy. Provided an anatomical space with few effector cells, tumor cells might use the bone marrow as a sanctuary site within which IS formation is infrequent. Insufficient selective pressure from effector cells might allow the regeneration of a newly resistant population of tumors cells that then repopulate other organs and accelerate systemic disease progression. This speculation is consistent with the clinical observation that patients under BiTE treatment often have relapses first detected in the bone marrow[25].

In conclusion, our study investigated the dynamics of IS formation under various conditions mimicking the heterogeneous nature of tumor microenvironments. To our knowledge, these theoretical models are the first to quantify the entire BiTE-induced IS formation process. The models reveal trajectories of tumor evolution through antigen escape across anatomical sites and have substantial implications for T cell-based immunotherapies.

Methods

Cell lines

Jurkat (Clone E6-1) and Raji cells were obtained from ATCC and maintained in RPMI1640 supplemented with 10–20% fetal bovine serum (FBS) and 1% penicillin-streptomycin. Cell lines were routinely tested to avoid mycoplasma contamination.

Cell sorting and antigen expression quantification

Cell populations with high (H), medium (M) and low (L) antigen expression were sorted based on natural expression levels, without any genetic engineering. PE-anti-CD3 and PE-anti-CD19 (BD Biosciences, San Jose, CA) were used as staining antibodies and BD FACSAria II was used to perform cell sorting. Surface expression of CD3 and CD19 were quantitatively determined by Quantum™ MESF beads (Bangs laboratories, Fishers, IN) and BD LSR II flow cytometry (Supplementary Fig. S1).

Cell co-incubation and imaging flow cytometry

Effector cell (E, Jurkat), target cell (T, Raji), and anti-hCD19-CD3 BiTE (BioVision, CA) were well mixed and co-incubated in 1 mL medium at 37 °C. CD3 or CD19 expression, drug concentration, cell density, E:T ratio, and duration of co-incubation varied as initial setups. After co-incubation, effector cell, target cell, actin, and nucleus were stained by FITC-anti-CD7 (eBiosciences, San Diego, CA), PE-anti-CD20 (BD Biosciences, San Jose, CA), AF647-anti-phalloidin (Thermo-Fisher, Waltham, MA) and DAPI, respectively. Staining for surface and intracellular markers was performed as described previously[26]. Samples were analyzed using Amnis ImageStream MKII (Luminex, Austin, TX). The frequency of IS was quantified using IDEAS (Luminex). The gating strategy is summarized in Supplementary Fig. S2.

Cell co-incubation under shear stress

To mimic the shear stress in blood circulation, effector cell, target cell, and antibody were well mixed in a circular pipe (internal diameter: 1.6 mm) and co-cultured (37 °C) at a certain flow velocity driven by a roller pump (Masterflex, Vernon Hills, IL). Flow velocities were adjusted to produce varying wall shear stresses, equivalent to those in the vein (1-6 dyn/cm^2), artery (10-24,

dyn/cm^2) and capillary (20-40 dyn/cm^2)[27-29]. After co-culture, sample staining and analysis were the same as previously described.

Modeling and simulation (base and in-vitro models)

Mechanistic agent-based models were developed to simulate IS formation dynamics in vitro and in vivo. We employed a sequential model-building strategy. First, we developed a model to capture IS formation dynamics within 1 hour, called the base model. The base model consisted of three modules at different dimensions: antibody-antigen binding (3D), cell-cell encounter, and cell-cell adhesion (2D) (Fig. 1b and 2).

Antibody-antigen binding to form binary complexes (BiTE-CD3 and BiTE-CD19) was considered a 3D process among free molecules. Rapid equilibrium was assumed. At specific total concentrations of CD3 (A), CD19 (B), and antibody (Y) in the co-incubation system, the equilibrium concentrations of free antigens ([A] and [B]) and binary complex ([AY] and [YB]) (Supplementary Fig. S3) were solved according to a model with two competing binding ligands[30]. Heterogeneous cell populations at equilibrium were generated by randomly assigning antigens and binary complexes to each individual cell (assign A and AY to effector cell, B and YB to target cell). The distribution of antigens and complexes on the cells (i.e., agents) were consistent with measured CD3 and CD19 expressions in respective cell lines (Supplementary Fig. S1 and Table S1).

CD3 down-regulation on effector cells was also considered in our model[31-36]. The rate of CD3 down-regulation was modeled as a function of surface binary complex ([AY]'), which was described by an empirical equation that reached steady state around 1 hour incubation, in line with literature (Supplementary Fig. S4). CD19 internalization was also introduced at a rate constant of 0.002/min[37,38]. Changes in surface antigen abundance ([A]', [AY]', and [YB]') for each cell was updated every 60 seconds in the model.

Encounters between effector and target cells are an essential step for IS formation. We adopted an approximate equation to determine the encounter probability of one effector cell meeting at least one target cell within a specific time, which is a function of the number of target cells in the system[15,39]. We assumed that effector cells diffuse independently, moving in Brownian motion, while target cells were immotile. For simplicity, the IS and IS variants were considered as a

singular moving cell entity when calculating the probability of encountering an additional free cell. Notably, spatial factors were considered in this encounter probability. The equations and parameters are provided in Supplementary Fig. S5; the spatial coefficients for different encounter scenarios are listed in Supplementary Table S1. Encounter probabilities were re-calculated every 60 seconds in the model due to the changing number of free cells over time.

When an effector cell physically contacts a target cell, it may have a chance to adhere or diffuse away. Cell-cell adhesion is mediated by ternary complexes (AYB) formed from binary complexes (AY or YB) and the availability of free antigen (B or A) on opposing cell surfaces (2D binding) (Supplementary Fig. S6). We assumed that stable adhesion relied on generating sufficient bonds within a short contact duration. Differential equations were used to simulate the number of bonds. The relationship between adhesion probability and the bond number was described by a modified deterministic equation (Supplementary Fig. S7)[40,41]. A higher number of bonds yielded a higher chance for engagements to result in an IS. The randomness arose from randomly assigned antigen expressions on both cells and contact duration (0.1-5 s). It is noteworthy that the "on" and "off" rate constants used in the equations are 2D kinetic constants on cellular membrane, which were derived from 3D rate constants by a "single-step model" (Supplementary Fig. S8)[14,42-44].

In the base model (time scale ≤ 1h), each free cell had only one chance to encounter in each round (60 seconds). Cells that failed to encounter or adhere would remain free cells in the next round. Newly formed IS would have a chance to encounter an additional free cell to form an IS variant in the next round (Fig. 2). Only one free cell was allowed to be added at each round. IS variant of up to four cells were allowed in the model. The algorithm for the base model is provided in Supplementary Fig. S9. Other important assumptions in the base model include: 1) no cell proliferation and death within the simulated time window; 2) no changes to the binding equilibrium between antibodies and antigens within 1 hour; 3) once formed, IS are not breakable.

Next, the in-vitro model was developed by incorporating serial cell engagement into the base model (Fig. 1b and 5a). The average duration of IS was assumed to be 150 min[8], and the detached effector cells from IS became free cells for additional IS formation. We made the following updates and assumptions to extend the time scale to 72 hours: 1) antibody-antigen binding equilibrium was recalibrated every hour; 2) CD19 internalization was ignored; 3) CD3 down-regulation for 1 hour and remained unchanged after; 4) antibody concentrations remained constant.

Clinical translation (in-vivo model)

Lastly, we expanded the model to develop the in-vivo model for simulating tumor-killing profiles in patients. Several additional modules, including multiple organ compartments and cell trafficking across organs, were defined in the in-vivo model (Fig. 1b and 6a).

In the in-vivo model, IS formation occurred within each organ-specific environment (Supplementary Table S2). Antibody concentrations and antigen expression (CD3 and CD19) in human T and B cells were estimated based on reported values[45-50]. The T and B cell densities at the organ level were derived based on the patient-specific blood cell numbers and the predefined "partition repertoire", which reflected the relative cell abundance between blood and each organ[17,51,52].

The cell trafficking rate was set at 4.17% per hour, which represents the fraction of B cells trafficking through the blood during a day relative to the total B cell in the system, in line with clinical data[17]. Each hour, 4.17% of B cells in all organs were randomly reassigned to a new location according to the pre-defined "partition repertoire" representing trafficking through the blood. T cell trafficking was not modeled, as T cell death was ignored. B cell turnover and changes in BiTE dose and organ T cell densities over time were allowed (Supplementary Table S2,3).

As the model output, blood B cell levels after treatment were derived from the residual B cells in organs based on the pre-defined "partition repertoire".

Data source and software

Publicly available clinical data[18,19,53-55] were digitized form the literature using WebPlot Digitizer. Simulation, plotting, and statistical analysis were implemented in R (3.6.0).

Acknowledgements

We thank Amgen Inc. for kindly sharing blinatumomab to support our pilot study.

Funding Source

National Institute of Health, R35GM119661

Author Contributions

Conceptualization: C.L., and Y.C.; methodology: C.L., S.K., and Y.C.; formal analysis: C.L., Y.C.; investigation: C.L., J.Z., and Y.C.; writing-original draft: C.L., and Y.C.; writing-reviewing and editing: C.L., S.K., J.Z., T.Q., T.D., and Y.C.; supervision: Y.C.; funding acquisition: Y.C.

Competing interests

T.Q. is a contractor for Hatteras Venture Partners and Y.C. is a consultant for Janssen Research & Development. No further competing interest was declared by other authors.

References

1. Nagorsen D., Kufer, P., Baeuerle P. A. & Bargou R. Blinatumomab: a historical perspective. *Pharmacol. Ther.* **136***,* 334-342 (2012).

2. Thakur, A., Huang, M. & Lum, L. G. Bispecific antibody based therapeutics: strengths and challenges. *Blood Rev.* **32**, 339-347 (2018).

3. Topp, M. S. et al. Phase II trial of the anti-CD19 bispecific T cell-engager blinatumomab shows hematologic and molecular remissions in patients with relapsed or refractory B-precursor acute lymphoblastic leukemia. *J Clin. Oncol.* **32**, 4134-4140 (2014).

4. Delon J., Germain R. N. Information transfer at the immunological synapse. *Curr. Biol.* **10,** R923-933 (2000).

5. Roda-Navarro, P. & Álvarez-Vallina, L. Understanding the spatial topology of artificial immunological synapses assembled in T cell-redirecting strategies: a major issue in cancer immunotherapy. *Front Cell Dev. Biol.* **7**, 370 (2020).

6. Xiong, W. et al. Immunological synapse predicts effectiveness of chimeric antigen receptor cells. *Mol. Ther.* **26**, 963-975 (2018).

7. Finetti, F. & Baldari, C. T. The immunological synapse as a pharmacological target. *Pharmacol. Res.* **134**, 118-133 (2018).

8. Fousek, K. et al. CAR T-cells that target acute B-lineage leukemia irrespective of CD19 expression. *Leukemia* **35**, 75-89 (2021).

9. Dustin, M. L. & Cooper., J. A. The immunological synapse and the actin cytoskeleton: molecular hardware for T cell signaling. *Nat. Immunol.* **1**, 23-29 (2000).

10. Xiling, J. et al. Development of a target cell-biologics-effector cell (TBE) complex-based cell killing model to characterize target cell depletion by T cell redirecting bispecific agents. *MAbs* **10**, 876-889 (2018).

11. Schropp, J., Khot, A., Shah, D. K. & Koch, G. Target-mediated drug disposition model for bispecific antibodies: properties, approximation, and optimal dosing strategy. *CPT Pharmacometrics Syst. Pharmacol.* **8**, 177-187 (2019).

12. Betts, A. et al. A translational quantitative systems pharmacology model for CD3 bispecific molecules: application to quantify T cell-mediated tumor cell killing by P-Cadherin LP DART. *AAPS J.* **21**, 66 (2019).

13. Song, L. et al. Mechanistic prediction of first-in-human dose for bispecific CD3/EpCAM T-cell engager antibody M701, using an integrated PK/PD modeling method. *Eur. J Pharm. Sci.* **158**, 105584 (2021).

14. Bell, G. I. Models for the specific adhesion of cells to cells. *Science* **200**, 618-627 (1978).

15. Celli, S. et al. How many dendritic cells are required to initiate a T-cell response? *Blood* **120**, 3945-3948 (2012).

16. Rogala, B. et al. Blinatumomab: enlisting serial killer T-cells in the war against hematologic malignancies. *Expert Opin. Biol. Ther.* **15**, 895-908 (2015).

17. Westermann, J. & Pabst, R. Distribution of lymphocyte subsets and natural killer cells in the human body. *Clin. Investig.* **70**, 539-544 (1992).

18. Zhu, M. et al. Blinatumomab pharmacodynamics and exposure-response relationships in relapsed/refractory acute lymphoblastic leukemia. *J Clin. Pharmacol.* **58**, 168-179 (2018).

19. Zugmaier, G. et al. Long-term survival and T-cell kinetics in relapsed/refractory ALL patients who achieved MRD response after blinatumomab treatment. *Blood*. **126**, 2578-2584 (2015).

20. Viardot, A. & Bargou, R. Bispecific antibodies in haematological malignancies. *Cancer Treat Rev*. **65**, 87-95 (2018).

21. Topp, M. S. et al. Safety and activity of blinatumomab for adult patients with relapsed or refractory B-precursor acute lymphoblastic leukaemia: a multicentre, single-arm, phase 2 study. *Lancet Oncol.* **16**, 57-66 (2015).

22. Eugene, F. et al. A comprehensive mathematical model for three-body binding equilibria. *J Am. Chem. Soc.* **135**, 6092-6099 (2013).

23. Arthur, V. et al. Predicting tumor killing and T-cell activation by T-cell bispecific antibodies as a function of target expression: combining in vitro experiments with systems modeling. *Mol. Cancer Ther.* **20**, 357-366 (2020).

24. Aldoss, I. et al. Correlates of resistance and relapse during blinatumomab therapy for relapsed/refractory acute lymphoblastic leukemia. *Am. J Hematol.* **92**, 858-865 (2017).

25. Locatelli, F. et al. Blinatumomab in pediatric relapsed/refractory B-cell acute lymphoblastic leukemia: RIALTO expanded access study final analysis. *Blood Adv.* **6**, 1004-1014 (2022).

26. Liu, C., He H., Li, X., Su, M. A. & Cao, Y. Dynamic metrics-based biomarkers to predict responders to anti-PD-1 immunotherapy. *Br. J Cancer* **120**, 346-355 (2019).

27. Kamiya, A., Bukhari, R. & Togawa, T. Adaptive regulation of wall shear stress optimizing vascular tree function. *Bull. Math. Biol.* **46**, 127-137 (1984).

28. Papaioannou, T. G. & Stefanadis, C. Vascular wall shear stress: basic principles and methods. *Hellenic J Cardiol.* **46**: 9-15 (2005).

29. Sebastian, B. & Dittrich, P. S. Microfluidics to mimic blood flow in health and disease. *Annu. Rev. Fluid Mech.* **50**, 483-504 (2018).

30. Yan, X., Chen, Y. & Krzyzanski, W. Methods of solving rapid binding target-mediated drug disposition model for two drugs competing for the same receptor. *J Pharmacokinet. Pharmacodyn.* **39**, 543-560 (2012).

31. Lanzavecchia, A., Iezzi, G. & Viola, A. From TCR engagement to T cell activation: a kinetic view of T cell behavior. *Cell* **96**, 1-4 (1999).

32. Valitutti, S., Müller, S., Cella, M., Padovan, E. & Lanzavecchia, A. Serial triggering of many T-cell receptors by a few peptide-MHC complexes. *Nature* **375**, 148-151 (1995).

33. San José, E., Borroto, A., Niedergang, F., Alcover, A. & Alarcón, B. Triggering the TCR complex causes the downregulation of nonengaged receptors by a signal transduction-dependent mechanism. *Immunity* **12**, 161-170 (2000).

34. Utzny, C., Coombs, D., Müller, S. & Valitutti, S. Analysis of peptide/MHC-induced TCR downregulation: deciphering the triggering kinetics. *Cell Biochem. Biophys.* **46**, 101-111 (2006).

35. Sousa, J., & Carneiro, J. A mathematical analysis of TCR serial triggering and down-regulation. *Eur. J Immunol.* **30**, 3219-3227 (2000).

36. Viola, A. et al. Quantitative contribution of CD4 and CD8 to T cell antigen receptor serial triggering. *J Exp. Med.* **186**, 1775-1779 (1997).

37. Du, X., Beers, R., Fitzgerald, D. J. & Pastan, I. Differential cellular internalization of anti-CD19 and -CD22 immunotoxins results in different cytotoxic activity. *Cancer Res.* **68**, 6300-6305 (2008).

38. Ingle, G. S. et al. High CD21 expression inhibits internalization of anti-CD19 antibodies and cytotoxicity of an anti-CD19-drug conjugate. *Br. J Haematol.* **140**, 46-58 (2008).

39. Miller, M. J., Wei, S. H., Cahalan, M. D. & Parker, I. Autonomous T cell trafficking examined in vivo with intravital two-photon microscopy. *Proc. Natl. Acad. Sci. USA*. **100**, 26049 (2003).

40. Chesla, S. E., Selvaraj, P. & Zhu, C. Measuring two-dimensional receptor-ligand binding kinetics by micropipette. *Biophys. J* **75**, 1553-1572 (1998).

41. Huang, J. et al. The kinetics of two-dimensional TCR and pMHC interactions determine T-cell responsiveness. *Nature* **464**, 932-936 (2010).

42. Faro, J., Castro, M. & Molina-París, C. A unifying mathematical framework for experimental TCR-pMHC kinetic constants. *Sci. Rep.* **7**, 46741 (2017).

43. Jansson, A. A mathematical framework for analyzing T cell receptor scanning of peptides. *Biophys. J* **99**, 2717-2725 (2010).

44. Dreier, T. et al. Extremely potent, rapid and costimulation-independent cytotoxic T-cell response against lymphoma cells catalyzed by a single-chain bispecific antibody. *Int. J Cancer* **100**, 690-697 (2002).

45. Xiling, J. et al. Development of a minimal physiologically-based pharmacokinetic/pharmacodynamic model to characterize target cell depletion and cytokine release for T cell-redirecting bispecific agents in humans. *Eur. J Pharm. Sci.* **146**, 105260 (2020).

46. Ginaldi, L. et al. Differential expression of CD3 and CD7 in T-cell malignancies: a quantitative study by flow cytometry. *Br. J Haematol.* **93**, 921-927 (1996).

47. Haso, W. et al. Anti-CD22-chimeric antigen receptors targeting B-cell precursor acute lymphoblastic leukemia. *Blood* **121**, 1165-1174 (2013).

48. Ginaldi, L. et al. Levels of expression of CD19 and CD20 in chronic B cell leukaemias. *J Clin. Pathol.* **51**, 364-369 (1998).

49. Rosenthal, J. et al. Heterogeneity of surface CD19 and CD22 expression in B lymphoblastic leukemia. *Am. J Hematol.* **93**, E352-E355 (2018).

50. Ramakrishna, S. et al. Modulation of target antigen density improves CAR T-cell functionality and persistence. *Clin. Cancer Res.* **25**, 5329-5341 (2019).

51. Hall, C., Lueshen, E., Mosat, A. & Linninger, A. A. Interspecies scaling in pharmacokinetics: a novel whole-body physiologically based modeling framework to discover drug biodistribution mechanisms in vivo. *J Pharm Sci.* **101**, 1221-1241 (2012).

52. Hassan, H. T. & El-Sheemy, M. Adult bone-marrow stem cells and their potential in medicine. *J R Soc. Med.* **97**, 465-471 (2004).

53. Bargou, R. et al. Tumor regression in cancer patients by very low doses of a T cell-engaging antibody. *Science* **321**, 974-977 (2008).

54. Zhu, M. et al. Blinatumomab, a bispecific T-cell engager (BiTE) for CD-19 targeted cancer immunotherapy: clinical pharmacology and its implications. *Clin. Pharmacokinet.* **55**, 1271-1288 (2016).

55. Klinger, M. et al. Immunopharmacologic response of patients with B-lineage acute lymphoblastic leukemia to continuous infusion of T cell-engaging CD19/CD3-bispecific BiTE antibody blinatumomab. *Blood* **119**, 6226-6233 (2012).